The Astrophysical Journal, 657:302–307, 2007 March 1

INVERSE COMPTON SCENARIOS FOR THE TeV GAMMA-RAY EMISSION OF THE GALACTIC CENTER

J. A. Hinton
Max-Planck-Institut für Kernphysik, Heidelberg; and Landessternwarte, Universität Heidelberg, Königstuhl, Heidelberg, Germany; and School of Physics and Astronomy, University of Leeds, Leeds, UK

and

F. A. Aharonian
Max-Planck-Institut für Kernphysik, Heidelberg, Germany; and Dublin Institute for Advanced Studies, Dublin, Ireland
Received 2006 July 25; accepted 2006 October 14

ABSTRACT

The intense Compton cooling of ultrarelativistic electrons in the Klein-Nishina regime in radiation-dominated environments, such as that found in the Galactic center, may result in radically different electron spectra than those produced by synchrotron cooling. We explore these effects and their impact on the X-ray and γ-ray spectra produced in electron accelerators in this region in comparison to elsewhere in our Galaxy. We discuss the broadband emission expected from the newly discovered pulsar wind nebula G359.95−0.04 and the possible relationship of this X-ray source to the central TeV γ-ray source HESS J1745−290. Finally, we discuss the possible relationship of the Galactic center *INTEGRAL* source IGR J1745.6−2901 to the TeV emission.

Subject headings: Galaxy: center — radiation mechanisms: nonthermal — X-rays: individual (G359.95−0.04)

Online material: color figures

1. INTRODUCTION

The detection of TeV γ-rays from the Galactic center (GC) by several groups, including Kosack et al. (2004), Tsuchiya et al. (2004), Aharonian et al. (2004b), and Albert et al. (2006), can be considered one of the most exciting discoveries of recent years in high-energy astrophysics. After initial disagreements, the basic properties of the TeV source (HESS J1745−290) now seem to be firmly established, with the values from the High Energy Stereoscopic System (HESS; Hinton 2004) providing the highest level of accuracy. The key experimental findings are as follows:

1. The energy spectrum in the range 0.15–20 TeV can be described by a power law: $dN/dE = k(E/1\ \mathrm{TeV})^{-\Gamma}\ \mathrm{cm}^{-2}\ \mathrm{s}^{-1}\ \mathrm{TeV}^{-1}$, with $k = 1.8 \pm 0.1_{\mathrm{stat}} \pm 0.3_{\mathrm{sys}}$ and $\Gamma = 2.29 \pm 0.05_{\mathrm{stat}} \pm 0.1_{\mathrm{sys}}$ (Rolland & Hinton 2005).
2. There is no evidence for variability on timescales of hours to years (Rolland & Hinton 2005; Albert et al. 2006).
3. The centroid of the γ-ray emission lies within $1'$ of Sgr A* (Aharonian et al. 2004b; Rolland & Hinton 2005).
4. The rms size of the emission region must be less than $3'$, equivalent to 7 pc at the GC distance (Aharonian et al. 2004b).

The implied 1–10 TeV γ-ray luminosity of the source is 10^{35} ergs s^{-1}. A wide range of possible counterparts and mechanisms have been put forward to explain the γ-ray emission. These include the annihilation of dark matter (unlikely due to the measured spectral shape; see Profumo 2005) and the astrophysical objects Sgr A* (Aharonian & Neronov 2005) and Sgr A East (Fatuzzo & Melia 2003; Crocker et al. 2005). A hadronic origin of the γ-ray emission seems plausible, originating either within these sources or indirectly via the injection of hadrons into the dense central parsec region (Aharonian & Neronov 2005; Lu et al. 2006; Liu et al. 2006). Indeed, there is strong evidence for the existence of a proton accelerator close to the GC (at least in the past) in the form of the recently discovered TeV emission of the giant molecular clouds (GMCs) of the central molecular zone (Aharonian et al. 2006). Nevertheless, an origin of the central $\leq 0.1^\circ$ γ-ray emission in the interactions of TeV electrons remains a compelling alternative. Several scenarios have been discussed in which the persistent TeV emission is explained by inverse Compton (IC) scattering of electrons in the central parsec. The termination shock of a hypothetical wind from the supermassive black hole (Atoyan & Dermer 2004), stellar wind shocks (Quataert & Loeb 2005), and the newly discovered X-ray nebulae $8''$ from Sgr A* (Wang et al. 2006) have all been proposed as acceleration sites for these electrons.

While the formation of synchrotron and IC nebulae around sources of multi-TeV electrons proceeds in general in the GC as in other regions of the Galactic disk (GD), the very high density of low-frequency radiation in the GC leads to significant deviations from the typical disk scenario. The high radiation density (out to $\sim$10 pc from Sgr A*) not only provides copious targets for γ-ray production, but also creates rather unusual conditions for the formation of the spectrum of TeV electrons. For magnetic fields less than $\sim$100 μG, the energy density of the radiation appears to be much higher than the energy density of the magnetic field; thus, even in the modest Klein-Nishina (KN) regime, TeV electrons are cooled predominantly by IC losses. This leads to *hardening* of the spectrum (not steepening, as in the typical GD environment) up to very high ($\geq$100 TeV) energies (the deep KN regime), where the synchrotron losses start to dominate over IC losses. Figure 1 illustrates the cooling time for electrons in the presence of both strong radiation fields and magnetic fields (*bottom*) and the modification of the injected electron spectrum after cooling (*top*). The time evolution of the electron spectrum (in Fig. 1 and throughout this paper) is calculated numerically, considering energy losses and injection of electrons in time steps much shorter than the age of the system. Synchrotron and IC energy losses are calculated using the formalism developed by Blumenthal & Gould (1970).

The irregular spectral shape of the electrons shown in Figure 1 is reflected differently in the synchrotron and IC radiation components (see, e.g., Khangulyan & Aharonian 2005; Moderski et al. 2005). Another interesting feature of these conditions is that due to enhanced IC losses, the synchrotron radiation of electrons will be strongly suppressed (by an order of magnitude or more), unless the magnetic field in extended regions of the GC exceeds 100 μG.

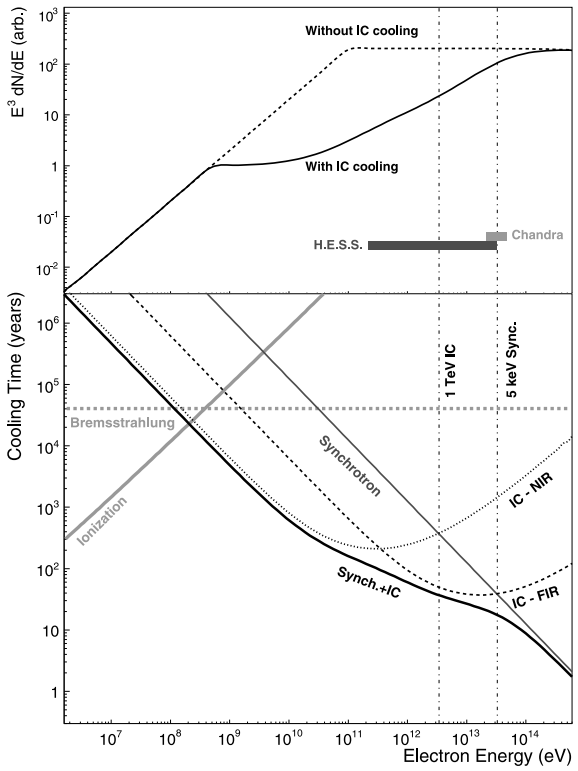

FIG. 1.—*Top*: Energy spectrum of electrons with continuous injection with $dN/dE \propto E^{-\alpha}$ (with $\alpha = 2$) and cooling over a 10^4 yr period. The dashed line shows the cooled spectrum for electrons suffering only synchrotron losses (for $B = 100\ \mu$G). The solid line shows the spectrum after synchrotron and IC cooling on radiation fields typical of the central parsec of our Galaxy. The shaded regions show the range of electron energies contributing to signals seen in the energy ranges of the *Chandra* and HESS instruments. *Bottom*: Cooling time via IC (*dashed and dotted lines*; FIR and NIR radiation fields) and synchrotron radiation (*solid dark gray line*). The lower heavy solid line shows the overall cooling time for IC and synchrotron radiation. The approximate energy loss timescales for ionization and bremsstrahlung (in a neutral environment of number density 1000 cm^{-3}) are shown for comparison. [*See the electronic edition of the Journal for a color version of this figure.*]

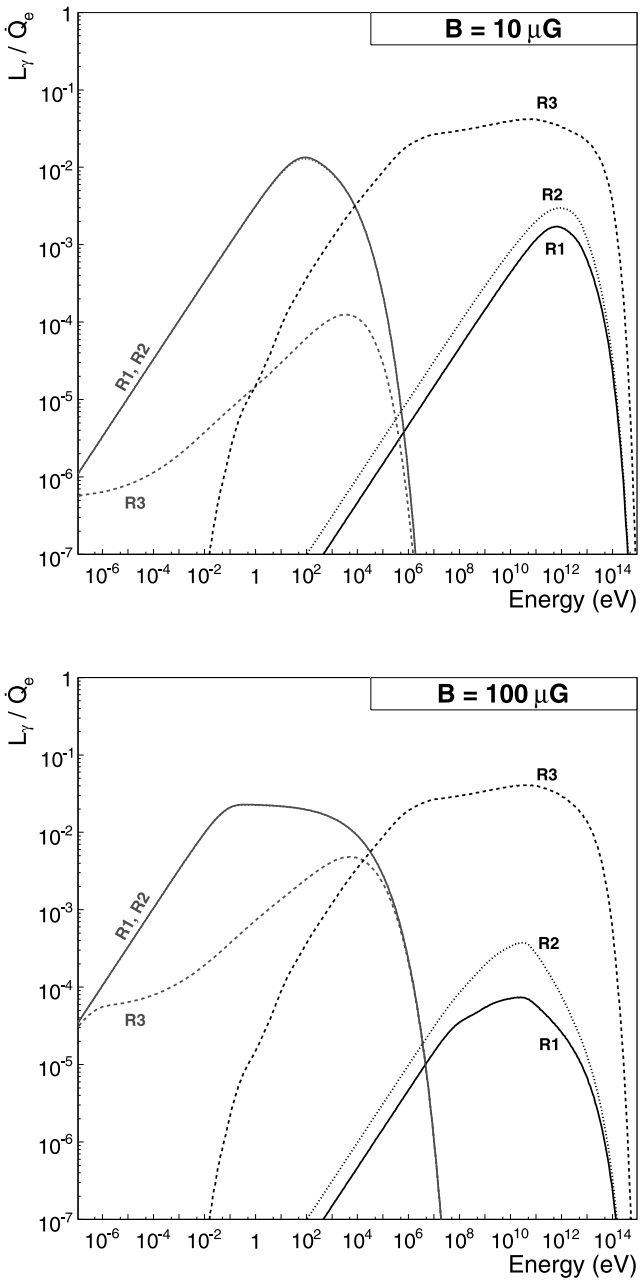

FIG. 2.—Fraction of the total power injected in electrons radiated in different spectral bands for $B = 10\ \mu$G (*top*) and $B = 100\ \mu$G (*bottom*). In each case three radiation fields are considered: R1, a typical Galactic disk environment; R2, ~100 pc from the GC; and R3, within the central parsec. Continuous injection (over a 10^4 yr period) with $dN/dE \propto E^{-2}$ and an exponential cutoff at 100 TeV are assumed in all cases. The synchrotron curve for R2 lies underneath that of R1. [*See the electronic edition of the Journal for a color version of this figure.*]

This situation is in stark contrast to that in the GD, where IC emission is strongly suppressed for magnetic fields >10 μG. In Figure 2, we compare the fractional energy distribution resulting from the injection of the same power-law spectrum of the electrons for two values of the mean magnetic field in the source (10 μG and 100 μG) for three locations in our Galaxy: (1) the central 1 pc, (2) at 100 pc from the GC, and (3) in a standard site in the GD. The radiation fields used in Figure 2 and throughout this paper are given in Table 1.

Some of these effects have been discussed by Wang et al. (2006) in the context of a possible identification of HESS J1745−290 with the candidate pulsar wind nebula (PWN) G359.95−0.04. In this paper, we present the results of numerical calculations based on a time-dependent treatment of the formation of the energy spectrum of the electrons. We discuss the case of G359.95−0.04 and show that indeed, this PWN can explain the TeV γ-ray emission from the GC. The implied B field in this scenario appears to be around 100 μG. Remarkably, PWNe similar to G359.95−0.04 (i.e., with similarly large B fields and comparable energetics) located in the conventional sites within the GD would be undetectable with any current or planned TeV γ-ray instrument. The converse also holds: typical TeV γ-ray PWNe (with B fields of ~10 μG or less) would not be detectable in X-rays if they were located in the central 1 pc region. Finally, we discuss the conditions implied by the interpretation of the hard X-ray emission detected by *INTEGRAL* (Neronov et al. 2005; Bélanger et al. 2006) as synchrotron emission of multi-TeV electrons in the context of the severe IC losses of these electrons.

2. PULSAR WIND NEBULAE

Pulsar wind nebulae are perhaps the most efficient astrophysical particle accelerators in our Galaxy. The best-studied PWN, the Crab Nebula, accelerates electrons up to ~10^{16} eV despite the rapid synchrotron losses of these particles in its 160 μG magnetic field (Aharonian et al. 2004a). The recent detections of extended TeV emission from several PWNe, including the detections of MSH 15−5-02 (Aharonian et al. 2005b) and G18.0−0.7/HESS J1825−137 (Aharonian et al. 2005c) with the HESS instrument,

TABLE 1
Energy Densities of the Thermal Components of Radiation Fields

Rad. Field	Component (kT) UV/Optical (3 eV)	NIR (0.3 eV)	FIR (6×10^{-3} eV)	CMBR (2.35×10^{-4} eV)
R1	...	0.2	0.2	0.26
R2	...	9	1	0.26
R3	5000	5000	500	0.26
R4	50	50	5	0.26

Notes.—The energy density is in units of eV cm^{-3}. The fields were used for the calculation of electron cooling and γ-ray production via inverse Compton scattering. Field R1 represents the typical Galactic disk environment. Field R2 reflects the situation in the inner $\sim$100 pc. Field R3 is a model of the intense field of the central cubic parsec of our Galaxy. Field R4 is a scaled-down version of field R3 that approximates the situation 10 pc from the GC.

suggest that such objects are copious TeV γ-ray emitters. In this context, a PWN may provide a natural explanation for the GC TeV emission. Here we discuss, in detail, the case of the new PWN candidate G359.95$-$0.04.

2.1. *The Case of G359.95$-$0.04*

The X-ray nebula G359.95$-$0.04 was discovered in deep *Chandra* observations of the Galactic center (Wang et al. 2006) and lies at a projected distance to Sgr A* of 0.3 pc. The nebula exhibits a cometary morphology with a projected size of 0.07 pc $\times$ 0.3 pc. The overall energy spectrum of this object is purely nonthermal, with a power-law index of $1.94^{+0.17}_{-0.14}$ and an unabsorbed 2–10 keV X-ray luminosity of $\approx 10^{34}$ ergs s^{-1}. The *Chandra* data reveal a softening of the spectral index with distance from the "head" of the nebula, a possible signature of cooling of the electrons away from the accelerator. Wang et al. (2006) have suggested that the head of the nebula contains a young pulsar and that G359.95$-$0.04 is likely a ram pressure–confined PWN.

G359.95$-$0.04 lies within the 68% confidence error circle of the γ-ray source HESS J1745$-$290. The possible connection between these two objects was pointed out by Wang et al. (2006), who discuss in some detail the important physical aspects involved in the relationship between the X-ray and γ-ray emission. One of our aims here is to make a full time-dependent calculation to investigate more deeply the likelihood of an association of these two objects. A major difficulty with such an association is the $\sim 0.1^\circ$ angular resolution of HESS. In this scenario, the γ-ray signal would be pointlike and nonvariable, and the only available information for modeling is the spectral data in the X-ray and γ-ray bands. However, the X-ray morphology provides some clues to the environment of the PWN. For example, the fact that the X-ray spectrum softens rather than hardens farther away from the (nominal) pulsar position indicates that the X-ray–emitting electrons are cooled by synchrotron radiation (or IC radiation in the Thompson regime) rather than by IC radiation in the Klein-Nishina regime, as might be expected in the dense GC radiation fields. This fact alone places a lower limit on the magnetic field in the PWN of ~ 100 μG.

Due to KN suppression, it is likely that the dominant target for IC radiation at a few TeV is the far-infrared background. Matching the flux of HESS J1745$-$290 at these energies with a nominal FIR radiation energy density of 5000 eV cm^{-3} (Davidson et al. 1992) requires a B field of ≈ 105 μG. In the case that HESS J1745$-$290 and G359.95$-$0.04 are *not* associated, this value provides a lower limit on the average magnetic field in the PWN. Figure 3 shows a model spectral energy distribution (SED) for G359.95$-$0.04 with IC on a FIR field. The injection spectrum

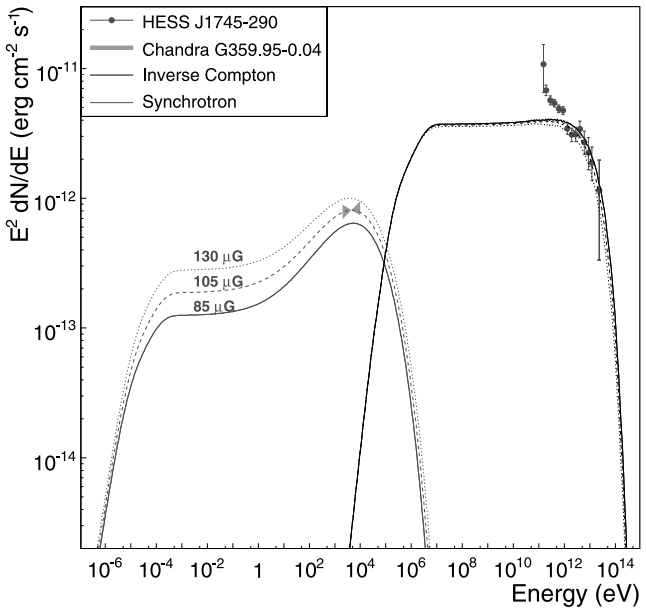

Fig. 3.—Spectral energy distribution for inverse Compton scattering on a single-temperature FIR radiation field of density 5000 eV cm^{-3}. The three line styles indicate the effect of changing the magnetic field strength (with all other parameters fixed). The assumed injection spectrum is described in the main text. HESS data are taken from Rolland & Hinton (2005), and *Chandra* data are from Wang et al. (2006). [*See the electronic edition of the Journal for a color version of this figure.*]

of the electrons is assumed to begin at 1 GeV and be of the form $dN/dE \propto E^{-\alpha} e^{-E/E_0}$, with $\alpha = 2$ and $E_0 = 100$ TeV. A source age of 10^4 yr is assumed, and a total power of 6.7×10^{35} ergs s^{-1} injected into relativistic electrons is required to match the measured X-ray flux (assuming a distance to the Galactic center of 7.6 ± 0.4 pc; Eisenhauer et al. 2005). As the cooling time of the electrons responsible for the observed X-ray and γ-ray emission is much shorter than the age of the pulsar in this scenario, possible evolutionary effects on the injection power (related to the breaking of the pulsar spin) can safely be neglected. We therefore assume a constant injection rate in the simulations presented here. Figure 3 demonstrates an important aspect of IC cooling: the KN effect acts twice on the IC spectrum (initially by distortion of the electron spectrum through cooling, and secondly in the production of IC emission), but only once on the synchrotron spectrum. This means that the hardening effect of cooling in the KN regime is masked in the IC spectrum but is clearly visible in the synchrotron emission.

The effect of adding different temperature components to the GC radiation field is shown in Figure 4. Near-infrared ($kT = 0.3$ eV) and ultraviolet ($kT = 3.0$ eV) energy densities of 5×10^4 eV cm^{-3} are assumed, consistent with the values expected within the central parsec of our Galaxy (Davidson et al. 1992). The injected electron spectrum is identical to that in Figure 3. In such a compound field, low-energy electrons are cooled by IC scattering on optical seed photons, with higher energies cooled by IC on the FIR. This effect leads to rather different shapes for the IC spectra from these two components. It can be seen in this figure that the contribution of the UV is likely to be small because of strong KN suppression. This optical/UV domain can in principle be explored by the *GLAST* satellite (Thompson 2004), but such measurements may be rather difficult due to the strong diffuse background and the modest angular resolution of the instrument. As is clear from Figure 1, bremsstrahlung losses are unlikely to be important in the PWN, as the ambient density is likely $\ll 1000$ cm^{-3}.

The spectral and spatial distribution of low-energy electrons in the PWN can in principle be traced using radio observations.

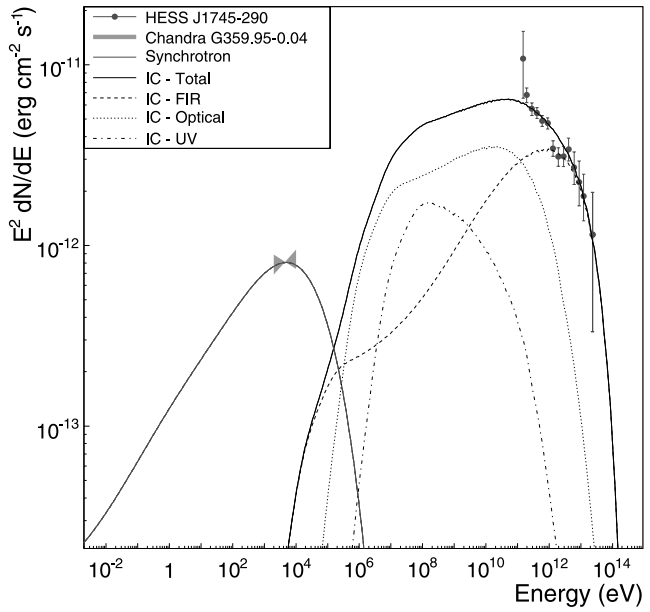

FIG. 4.—Spectral energy distribution for a realistic GC radiation field with FIR, optical, and UV components. The magnetic field strength is fixed at 105 μG. Details are given in the text. [*See the electronic edition of the Journal for a color version of this figure*.]

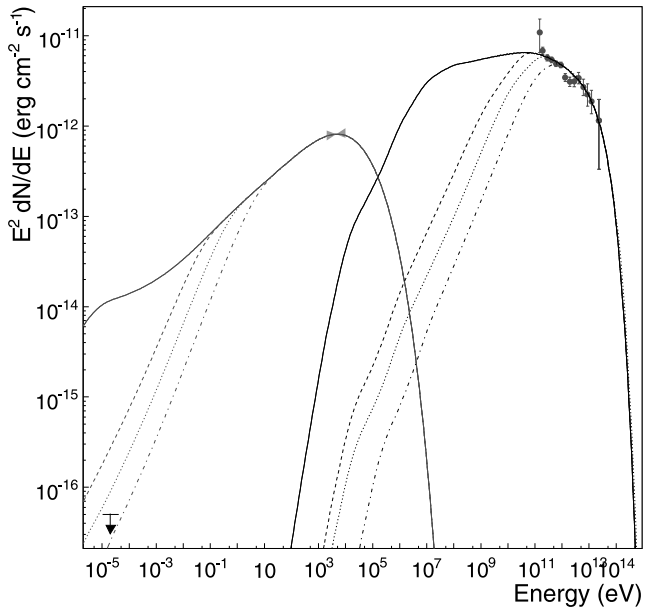

FIG. 5.—Same as Fig. 4, but showing the effect of a low-energy cutoff in the injected electron spectrum (and with an expanded flux scale). The corresponding minimum energies are 1 MeV (*solid line*), 100 GeV (*dashed line*), 300 GeV (*dotted line*), and 1 TeV (*dot-dashed line*). A 6 cm radio flux upper limit for G359.95−0.04 from F. Yusef-Zadeh (2006, private communication) is also shown. [*See the electronic edition of the Journal for a color version of this figure*.]

However, no pointlike or extended source is observed at the position of G359.95−0.04 in 6 cm observations, and a 3 σ energy flux upper limit of 5×10^{-17} ergs cm^{-2} s^{-1} has been derived (F. Yusef-Zadeh 2006, private communication). This limit lies almost 3 orders of magnitude below the curve shown in Figure 3. There are two factors that may both act to mitigate this apparent contradiction:

1. The electron energy spectrum has a low-energy cutoff. Figure 5 shows the impact of a low-energy cutoff in the electron spectrum on the IC and synchrotron spectra. If the radio emission region is considered to be identical to that of the keV X-rays (see below), then there is an implied low-energy cutoff at $\sim$1 TeV and a rather poor agreement with the lowest energy γ-ray data points. Indeed, a low-energy cutoff in the electron spectrum is expected within the PWN paradigm. For example, in the case of the Crab Nebula, Kennel & Coriniti (1984) suggest a minimum injection energy of $\sim$1 TeV at the wind termination shock. Wang et al. (2006) suggested a minimum low-energy cutoff of 5 GeV, which they derived from the radio data available at that time.

2. The cooling time of the radio-emitting electrons is almost 3 orders of magnitude longer than that of the X-ray–emitting electrons. Depending on the transport mechanism of particles in the nebula, the angular diameter of the radio emission may be expected to be much larger than the X-ray nebula, and the radio emission may have a correspondingly lower surface brightness. We envisage two general transport scenarios, the first of which is energy-independent advection. In this case, the PWN size is inversely proportional to the cooling time of the electrons, the ratio of the radio–to–X-ray angular size is $\sim$1000, and the flux within the bounds of the X-ray nebula is a factor of 10^6 lower than that presented in Figures 4 and 5. Clearly, there is no contradiction to the radio limit in this case. The second scenario is diffusion, with $D \propto E^{\alpha}$ and $r = (2Dt)^{1/2}$. In this case, the PWN size is proportional to $(E^{\alpha}/t_{\rm cool})^{1/2}$. For a value of $\alpha = 0.5$, the expected ratio of the radio–to–X-ray size is $\sim$3 (implying a reduction of 1 order of magnitude in surface brightness). In this case a low-energy cutoff at $\sim$50 GeV is still required. Larger values of α (for example, Bohm diffusion, with $\alpha = 1$) appear to be excluded by the observed energy-dependent morphology at X-ray wavelengths.

Regardless of the nature of the TeV source, it seems that one or both of these effects must occur to explain the radio–to–X-ray behavior of G359.95−0.04.

Figure 1 (*top*) illustrates the electron energies contributing to the HESS and *Chandra* signals for a 100 μG magnetic field. As the γ-ray emission takes place predominantly in the KN regime, the energy range of the electrons probed by HESS is extended by an order of magnitude relative to the Thompson-regime case. In contrast, the narrow energy range probed by *Chandra* reflects the standard $\epsilon_{\gamma} \propto (\epsilon_e)^{1/2}$ case. As synchrotron emission below 1 keV is heavily absorbed in the GC, very high energy (VHE) γ-ray emission represents the *only* way to study the 200 GeV–20 TeV electrons. From the bottom panel of Figure 1, it is apparent that the X-ray–emitting electrons have extremely short lifetimes ($\sim$20 yr). This fact, coupled with the known projected size of the PWN in X-rays ($\sim$0.3 pc), implies that the propagation speed of electrons downstream from the pulsar should be $\sim$10% of the speed of light, consistent with expectations for PWNe (see, for example, Blondin et al. 2001 and Kennel & Coriniti 1984).

It is clear from Figure 4 that the shape of the HESS and *Chandra* spectra can be explained in broad terms in this scenario. G359.95−0.04 may produce $\sim$100 GeV γ rays very efficiently despite its high B field. Fine-tuning of the model and adjustment of the radiation fields would be required to fit all HESS spectral data points, but we consider such tuning unjustified, given the possibility of the contribution of other sources (the supernova remnant Sgr A East, Sgr A*, etc.) to the HESS signal and since there are larger systematic errors on the HESS spectrum close to threshold. It therefore appears that G359.95−0.04 is a promising counterpart to the TeV GC source. As can be seen from Figure 2, a PWN like G359.95−0.04 could not be detected by any current or planned γ-ray detector if it were located in a standard region of the Galactic disk. The existence of extended regions with comparable

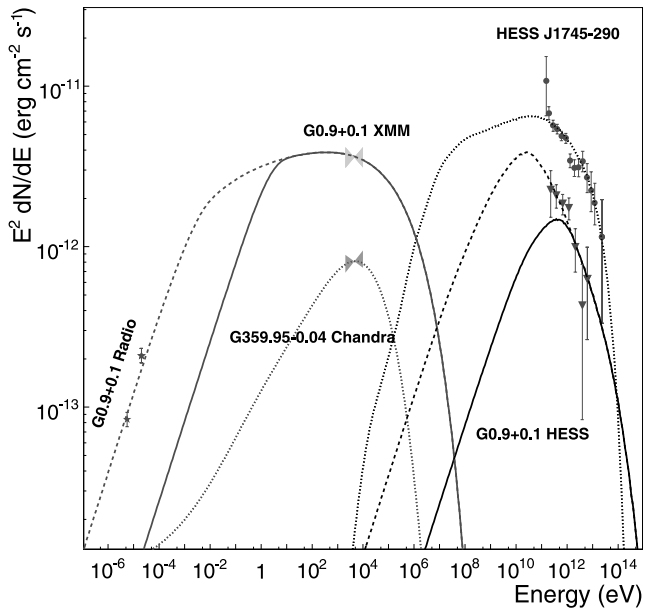

FIG. 6.—Comparison of the G359.95−0.04 SED shown in Fig. 4 (*dotted model curves*) with that of G0.9+0.1 (*solid and dashed curves*). The solid and dashed curves differ only in the assumed age of the source. Model parameters are given in the text. Radio data are taken from Helfand & Becker (1987), and *XMM-Newton* data are from Porquet et al. (2003). [*See the electronic edition of the Journal for a color version of this figure.*]

radiation densities outside of the GC (for example, in the central regions of young stellar clusters) seems unlikely, since ~1000 O stars would be required within 1 cubic parsec to reach this energy density.

2.2. *Comparison with G0.9+0.1*

G0.9+0.1 is a composite supernova remnant (SNR) with a bright radio shell and a compact core (Helfand & Becker 1987). The central object was identified as a PWN on the basis of its X-ray properties (Mereghetti et al. 1998; Porquet et al. 2003). VHE γ-ray emission associated with the PWN has been reported by the HESS collaboration (Aharonian et al. 2005a), with an energy flux comparable to that emitted in X-rays ($\sim 3 \times 10^{-12}$ cm^{-2} s^{-1}). The PWN in G0.9+0.1 can be considered an intermediate case between a "standard" disk PWN and G359.95−0.04. With a projected distance from the GC of 100 pc, radiation fields close to G0.9+0.1 are likely to be a factor of 10–100 higher than local densities, as represented by radiation field R2 in Table 1 (see, for example, Moskalenko et al. 2006). Indeed, an increased energy density of 8 eV cm^{-3} in optical photons was invoked in Aharonian et al. (2005a), in which a time-independent IC model[1] was fitted to the X-ray and γ-ray data. Here we revisit the SED of G0.9+0.1 from the perspective of a time-dependent evolution of the electron spectrum. In the following, we assume that G0.9+0.1 is located at the same distance as the GC (7.6 kpc).

Using values of the optical and FIR densities of 9 eV cm^{-3} and 1 eV cm^{-3}, respectively, as suggested by Moskalenko et al. (2006) for the wider GC region, we find that a model with $\alpha = 2$, $L_e = 7 \times 10^{36}$ ergs s^{-1}, $B = 10$ μG, and a pulsar age of 40 kyr is consistent with the HESS and X-ray data (see Fig. 6). This value is significantly larger than the 6800 yr age of the remnant estimated by assuming expansion in the Sedov phase (Mereghetti et al. 1998). Pulsar ages much shorter than 40 kyr are excluded by the absence of a spectral maximum (produced by a cooling break in the electron spectrum) within the HESS energy range. Recently, Porter et al. (2006) have fitted the "prompt" electron spectrum of G0.9+0.1 using the radiation field of Moskalenko et al. (2006) and derive a magnetic field of $B = 9.5$ μG, which is very close (as expected) to the value given here.

A second component of lower energy electrons is required to explain the radio emission (Helfand & Becker 1987) unless an age of $\approx 6 \times 10^5$ yr is assumed (see dashed lines in Fig. 6). Sidoli et al. (2000) used the break energy implied by the combination of radio and X-ray data to estimate the age of the pulsar to be ~3000 yr (assuming $B = 67$ μG). The much larger age derived here is a consequence of the lower magnetic field value established by the combination of X-ray and γ-ray data.

3. A CENTRAL 10 pc SOURCE

The recently detected hard (20–100 keV) X-ray source IGR J1745.6−2901 (Bélanger et al. 2004) is located within 1′ of Sgr A* and is coincident with HESS J1745−290. The angular resolution of *INTEGRAL* (12′ FWHM) is comparable with that of HESS, and similar difficulties exist with the identification of a counterpart. However, a combination of the *INTEGRAL* data with that of *XMM-Newton* suggests that the *INTEGRAL* source represents the sum of the emission of the central ~20 pc, either from a diffuse component or from the combination of several discrete sources (Neronov et al. 2005; Bélanger et al. 2006). The combined *XMM-Newton*/*INTEGRAL* X-ray spectrum of the central region has been derived by both groups, but with somewhat different results. Neronov et al. (2005) provide a broken power-law fit with $\Gamma_1 = 1.85^{+0.02}_{-0.06}$ and $\Gamma_2 = 3.3 \pm 0.1$, with a break at 26 ± 1 keV (hereafter the BPL fit). Bélanger et al. (2006) provide a broken power-law fit with $\Gamma_1 = 1.51^{+0.06}_{-0.09}$ and $\Gamma_2 = 3.22^{+0.34}_{-0.30}$, with a break at $27.1^{+2.8}_{-4.4}$ keV, and also a cutoff power-law fit: $\Gamma = 1.09^{+0.03}_{-0.05}$, with $E_{\rm cut} = 24.38^{+0.55}_{-0.76}$ keV (hereafter the PLEC fit). Of these three fits, BPL and PLEC represent the extremes and are used here to illustrate the impact of the X-ray spectral shape on the interpretation. If this emission has a synchrotron origin, then the broken power-law fit suggests a change in the electron spectral slope of ~3, which is incompatible with the effects of cooling or escape, and with standard acceleration scenarios. It therefore seems that the *INTEGRAL* data represent the end of the X-ray spectrum of this object or objects. Figure 7 shows approximate error boxes corresponding to the BPL and PLEC spectral fits. The difference in the low-energy slope of these two fits has important implications for the interpretation of this signal in a synchrotron scenario. In either case, an abrupt end to the electron spectrum is required to produce an exponential cutoff in the synchrotron spectrum. The PLEC fit implies an extremely hard electron spectrum.

Although considerable uncertainty exists in the radiation density ~10 pc from the GC, it seems likely that the average energy density within the 40 pc diameter *INTEGRAL* source is roughly 2 orders of magnitude lower than that within the central parsec (see, for example, Yusef-Zadeh et al. 1996). For the calculation of the inverse Compton emission, we therefore assume the radiation field R4 given in Table 1. With this radiation density, the association of HESS J1745−290 with IGR J1745.6−2901 implies a B field of ~100 μG. In the case that these objects are not associated, this B field can be considered as a lower limit on the mean value within the source or sources contributing to the *INTEGRAL* signal. Conversely, if the γ-ray emission has an inverse Compton origin within a 10 pc scale source, then the B field in this region must be <100 μG to avoid overproducing synchrotron emission. For a 100 μG magnetic field, 20 keV synchrotron photons are produced by ~70 TeV electrons. The cooling time of

[1] That is, a model for the present-day electron spectrum without consideration of the injection spectrum required to produce such a spectrum after cooling.

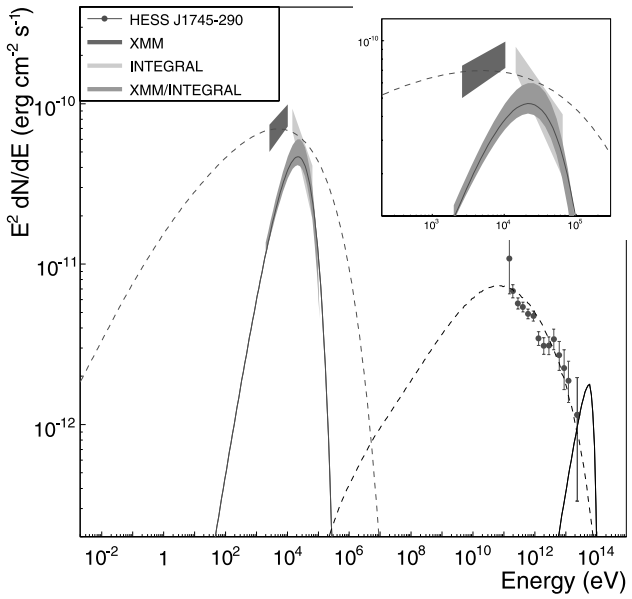

FIG. 7.—Spectral energy distribution for a central 10 pc *XMM-Newton*/*INTEGRAL*/HESS source. Separate *XMM-Newton* and *INTEGRAL* data are taken from Neronov et al. (2005), and the combined *XMM-Newton*/*INTEGRAL* fit is that of Bélanger et al. (2006). Model curves are shown for two scenarios: a very young source with $B = 50\,\mu$G, an electron spectrum with $\alpha = 0.3$, and a sharp cutoff at 100 TeV (PLEC; *solid curve*), and an old source with $B = 110\,\mu$G and an injection spectrum with $\alpha = 1.5$ and an exponential cutoff at 150 TeV (BPL; *dashed curve*). The inset panel provides an expanded view of the X-ray part of the SED. [*See the electronic edition of the Journal for a color version of this figure.*]

these electrons in such a field is extremely short ($\sim$18 yr). The time required for electrons to diffuse out of the central 10 pc is comparable ($\sim$10 yr) if a diffusion coefficient close to that appropriate for 70 TeV Galactic cosmic rays is assumed (i.e., $D \approx 6 \times 10^{30}$ cm^2 s^{-1}). It therefore seems rather difficult to produce a truly diffuse 20 pc source in the presence of such rapid energy losses. This cooling-time problem was previously discussed by Neronov et al. (2005). A model similar to that of Quataert & Loeb (2005), with acceleration occurring at stellar wind shocks, could avoid this problem by distributing the acceleration sites of electrons over the emission region.

Figure 7 shows two model curves illustrating the relationship between the X-ray and γ-ray emission. The first (*solid*) line matches the PLEC fit to the X-ray spectrum but can explain only the highest energy HESS points. This scenario requires both an extremely young source (to avoid a cooled spectrum in the *XMM-Newton* domain) and a very hard injection spectrum. The second curve (*dashed line*) is similar to that given in Neronov et al. (2005) and provides marginal agreement to the BPL fit and reasonable agreement with the HESS spectral data. The dramatic difference between these two scenarios illustrates the importance of better constraints on the X-ray spectrum and highlights the value of combined X-ray/γ-ray measurements.

4. SUMMARY

The central $\sim$10 pc of our Galaxy provides a unique environment in which high radiation energy densities lead to efficient inverse Compton γ-ray production and also, due to the Klein-Nishina effect, to substantial modifications to the form of the cooled electron spectra. This region appears to be the only location in our Galaxy in which pulsar wind nebulae with high magnetic fields and moderate spin-down luminosities can produce detectable γ-ray emission. In this context, the candidate PWN G359.95$-$0.04 provides a plausible counterpart to the γ-ray source HESS J1745$-$290. The interpretation of IGR J1745.6$-$2901 and HESS J1745$-$290 in terms of synchrotron/IC emission in a diffuse 20 pc source is difficult, due to the rapid energy losses of electrons in the region, but remains a viable alternative hypothesis. Finally, hadronic models for the TeV emission, while beyond the scope of this paper, provide equally viable explanations for the current experimental data. Improved γ-ray data should be available in the medium term from *GLAST* (Thompson 2004) and HESS. Phase 2 (Punch 2005) instruments will also provide important constraints on the origin of the high-energy emission.

J. A. H. acknowledges the support of the German BMBF through Verbundforschung Astro-Teilchenphysik (05CH5VH1/0). We are grateful to Farhad Yusef-Zadeh for providing a radio upper limit for G359.95$-$0.04. We would also like to thank Mitya Khangulyan for many useful discussions and Karl Kosack for his careful reading of the manuscript.

REFERENCES

Aharonian, F. A., & Neronov, A. 2005, Ap&SS, 300, 255
Aharonian, F. A., et al. 2004a, A&A, 425, L13
———. 2004b, ApJ, 614, 897
———. 2005a, A&A, 432, L25
———. 2005b, A&A, 435, L17
———. 2005c, A&A, 442, L25
———. 2006, Nature, 439, 695
Albert, J., et al. 2006, ApJ, 638, L101
Atoyan, A. M., & Dermer, C. D. 2004, ApJ, 617, L123
Bélanger, G., et al. 2004, ApJ, 601, L163
———. 2006, ApJ, 636, 275
Blondin, J. M., Chevalier, R. A., & Frierson, D. M. 2001, ApJ, 563, 806
Blumenthal, G. R., & Gould, R. J. 1970, Rev. Mod. Phys., 42, 237
Crocker, R. M., Fatuzzo, M., Jokipii, J. R., Melia, F., & Volkas, R. R. 2005, ApJ, 622, 892
Davidson, J. A., Werner, M. W., Wu, X., Lester, D. F., Harvey, P. M., Joy, M., & Morris, M. 1992, ApJ, 387, 189
Eisenhauer, F., et al. 2005, ApJ, 628, 246
Fatuzzo, M., & Melia, F. 2003, ApJ, 596, 1035
Helfand, D. J., & Becker, R. H., 1987, ApJ, 314, 203
Hinton, J. A. 2004, NewA Rev., 48, 331
Kennel, C. F., & Coriniti, F. V. 1984, ApJ, 283, 710
Khangulyan, D., & Aharonian, F. A. 2005, in AIP Conf. Proc. 745, 2nd Int. Symp. on High Energy Gamma-Ray Astronomy, ed. F. A. Aharonian, H. J. Völk, & D. Horns (New York: AIP), 359
Kosack, K., et al. 2004, ApJ, 608, L97
Liu, S., Melia, F., Petrosian, V., & Fatuzzo, M. 2006, ApJ, 647, 1099
Lu, Y., Cheng, K. S., & Huang, Y. F. 2006, ApJ, 641, 288
Mereghetti, S., Sidoli, L., & Israel, G. L. 1998, A&A, 331, L77
Moderski, R., Sikora, M., Coppi, P. S., & Aharonian, F. 2005, MNRAS, 363, 954
Moskalenko, I. V., Porter, T. A., & Strong, A. W. 2006, ApJ, 640, L155
Neronov, A., Chernyakova, M., Courvoisier, T. J.-L., & Walter, R. 2005, A&A, submitted (astro-ph/0506437)
Porquet, D., Decourchelle, A., & Warwick, R. S. 2003, A&A, 401, 197
Porter, T. A., Moskalenko, I. V., & Strong, A. W. 2006, ApJ, 648, L29
Profumo, S. 2005, Phys. Rev. D, 72, 103521
Punch, M. 2005, in Towards a Network of Atmospheric Cherenkov Detectors VII, ed. B. Degrange & G. Fontaine (Palaiseau: Ecole Polytechnique), 379
Quataert, E., & Loeb, A. 2005, ApJ, 635, L45
Rolland, L., & Hinton, J. A. 2005, Proc. 29th Int. Cosmic Ray Conf. (Pune), 4, 109
Sidoli, L., Mereghetti, S., Israel, G. L., & Bocchino, F. 2000, A&A, 361, 719
Thompson, D. J. 2004, NewA Rev., 48, 543
Tsuchiya, K., et al. 2004, ApJ, 606, L115
Wang, Q. D., Lu, F. J., & Gotthelf, E. V. 2006, MNRAS, 367, 937
Yusef-Zadeh, F., Wardle, M., & Roberts, D. 1996, ApJ, 458, L21